INDIVIDUAL SARCOMERE LENGTH DETERMINATION FROM ISOLATED CARDIAC CELLS USING HIGH-RESOLUTION OPTICAL MICROSCOPY AND DIGITAL IMAGE PROCESSING

KENNETH P. ROOS AND ALLAN J. BRADY
Department of Physiology and the American Heart Association, Greater Los Angeles Affiliate Cardiovascular Research Laboratory, University of California at Los Angeles, School of Medicine, Los Angeles, California 90024

ABSTRACT Discrete sarcomere lengths have been determined from dynamically contracting isolated cardiac cells with a high-speed, high-resolution direct optical imaging system. Calcium-tolerant cardiac cells from the rat are isolated by perfusion with collagenase and hyaluronidase. Individual sarcomere lengths can be determined by directly imaging the cell's striation pattern onto a solid-state charge-coupled device (CCD) detector interfaced with a digital computer. The precision of detection in a real light microscopic optical system is discussed in relation to the type of image detector, optical contrast enhancement techniques, and digital image processing. The optical performance of the direct striation pattern image apparatus has been determined empirically with test grids under standard bright-field and Nomarski–differential interference contrast (DIC) conditions for application to real muscle imaging. Discrete striation positions of isolated cells have been detected and followed with high precision during phasic contraction-relaxation cycles down to average sarcomere lengths as short as 1.43 $\pm$0.053 μm. The maximum rates of contraction and relaxation are rapid and synchronous in time course along the length of the cell. These results indicate that direct optical imaging can provide an accurate means to monitor discrete striations and sarcomere lengths along the length of Ca^{2+}-tolerant heart cells.

INTRODUCTION

The alternating light-dark banding pattern is the most striking feature of vertebrate striated muscle when observed through the light microscope. The banding pattern image arises directly from regional refractive index differences of the interdigitating thick and thin filaments (Huxley and Niedergerke, 1954; Huxley and Hanson, 1954). The anisotropic A bands formed by the interdigitated thick and thin filaments are more opaque and birefringent than the isotropic I bands from the thin filaments alone. Like most unstained biological tissue observed under standard bright-field light microscopy, a striated muscle image is of very low contrast. Apparent improved contrast can be achieved by stopping down—reducing—the microscope condenser's aperture, but only at the expense of a corresponding loss of spatial resolution. However, by utilizing the differential birefringence of the A and I bands with polarized light interference microscopy, high-contrast, high-resolution images of the muscle striation patterns can be obtained (Huxley and Niedergerke, 1958). Recent advances in the application of external detectors to microscopy and in video image enhancement techniques have revolutionized light microscopic imaging of small biological specimens (Allen et al., 1981 *a*; Allen et al., 1981 *b*; Inoué, 1981; and Walter and Burns, 1981).

Quantitative imaging leading to accurate measurement of A-I band spacing (i.e., sarcomere length) can provide important information about the relation of interfilament overlap and mechanical contractile performance (Huxley, 1957; Gordon et al., 1966; and Ford et al., 1977). The recent utilization of the laser light diffraction technique has greatly improved the precision of mean sarcomere length determination in skeletal (Cleworth and Edman, 1972; Paolini et al., 1977) and cardiac (Krueger and Pollack, 1975; Krueger et al., 1980) muscle preparations. However, sarcomere lengths determined from diffractometric analysis, are limited in that they represent an average value of only those sarcomeres transilluminated by the laser beam. Furthermore, the sources of the asymmetrical right-left diffraction pattern intensities and fine structure have yet to be defined satisfactorily (Rudel and Zite-Ferenczy, 1979; and Leung, in press). These limitations exclude the use of diffraction techniques when the quantification and eventual control of sarcomere length uniformity over the length of a muscle preparation are desired. Thus, a more discrete method of optical imaging must be used to quantify individual sarcomere lengths.

The Ca^{2+}-tolerant isolated cardiac cell preparation (myocyte) has shown much promise as an improved system for the study of cardiac muscle biochemistry, electrophysiology, and mechanical performance (Brady et al., 1979; Krueger et al., 1980; Powell et al., 1980; and Wittenberg and Robinson, 1981). The small size and functional integrity of this myocyte preparation make it ideally suited for study with a light microscope where the entire cell can be observed as a complete contractile unit. Fabiato and Fabiato (1976) and Fabiato (1981) in mechanically skinned and intact frog, dog, and rat cardiac cells, and Rieser et al. (1979) and DeClerck et al. (1981) in functionally skinned rabbit and rat cardiac cells, have all utilized light microscopes coupled to TV cameras as sarcomere length monitors.

We recently developed an approach to produce images of the striation patterns directly from the length of our Ca^{2+}-tolerant rat cardiac cells (Brady et al., 1979) using a phase-contrast microscope coupled to a solid-state photodiode detector and digital computer (Roos et al., 1982). Sarcomere lengths from isolated cells were examined at rest and at the peak of electrically paced phasic contractions over a range of osmotic conditions. These initial studies revealed several weaknesses in the implementation of, but not in the basic concept or practicality of, the direct-image approach for discrete striation measurement. Specifically, the phase contrast based optical system did not provide the optimal optical images necessary for discrete striation resolution. Furthermore, the temporal resolution of the computer data acquisition procedure was too slow to "freeze" striation patterns during dynamic contraction-relaxation cycling. Thus, the direct-image system was upgraded to obtain more accurate determinations of individual sarcomere lengths from resting and dynamically contracting isolated cardiac muscle cells by using high-resolution immersion optics with differential interference contrast (DIC), state of the art electronics, and improved digital image processing techniques. This manuscript outlines the upgraded direct image system, its capabilities and its limitations. The image performance characteristics of our optical system have been determined empirically from calibrated test grids and applied to the muscles' striation pattern data to provide a known basis for individual sarcomere length determination. Striation patterns have been sampled from contracting isolated heart cells and these patterns demonstrate the possibility of measurement of discrete sarcomere dynamics.

METHODS

Cell Preparation

Calcium-tolerant isolated cardiac cells (Fig. 1) were prepared from adult rat hearts by retrograde perfusion with collagenase and hyaluronidase as detailed previously (Brady et al., 1979; and Roos et al., 1982). Following digestion, the cells were dispersed from the minced tissue by gentle agitation in a Petri dish containing oxygenated Tyrode's phosphate solution (pH 7.2, in mM: NaCl, 110; KCl, 4; $NaHCO_3$, 10; $MgCl_2$, 1.0; NaH_2PO_4, 20.435; $CaCl_2$, 1.0) with a measured osmolarity of 290 ± 3 mOsm/Kg H_2O. After at least a 1 h equilibration period, an aliquot of cells was transferred to the imaging chamber of the microscope. Only cells that met the following criteria were used for imaging experiments: rodlike shape (average, 115 x 20 μm), distinct and ordered striation pattern, no discernible membrane disruption or blebs, and paced electrical excitability (no spontaneous wavelike contractions in millimolar Ca_o^{2+} concentrations).

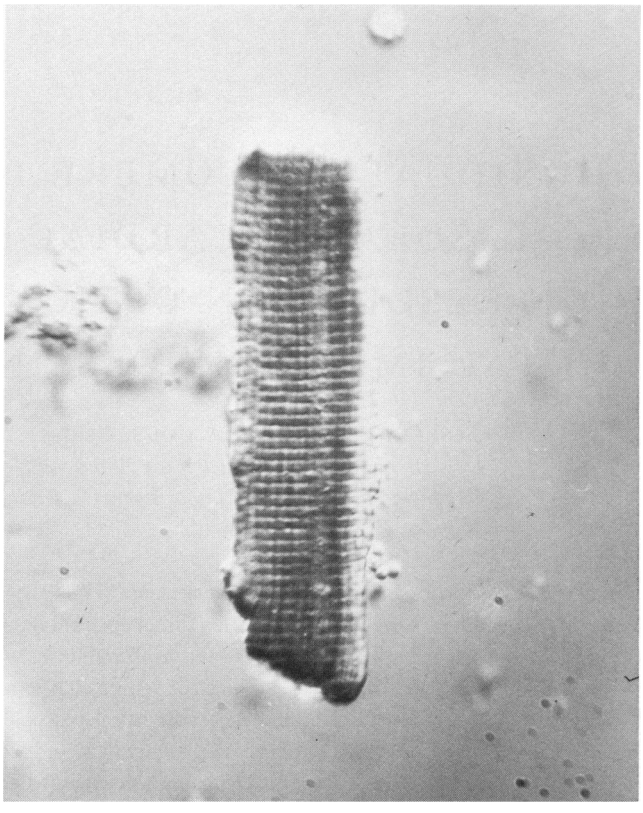

FIGURE 1 Photomicrograph. Nomarski DIC image of isolated cardiac cell photographed on Kodak TP2415 (Eastman Kodak Co., Rochester, NY) with a high extinction Wollaston prism bias compensation. The average sarcomere length is 1.87 ±0.08 μm.

Direct Image System

The direct image apparatus has been extensively modified to improve its spatial and temporal resolution over that of the previous design (Lubell and Roos, 1980; Roos et al., 1982). Fig. 2 schematizes the improved striation pattern imaging apparatus that is built around a Zeiss Standard microscope (Carl Zeiss, Inc., Thornwood, NY) fitted with Normarski-type differential interference contrast (DIC) immersion optics and a modified PDP 11/34a minicomputer (Digital Equipment Corp., Maynard, MA). High-intensity white light produced from a Xenon arc source passes through several heat filters, a polarizer, and DIC oil immersion condenser (numerical aperture (NA) = 1.4) to transilluminate the selected isolated cardiac cells in the imaging chamber built onto the stage of the microscope. An image of the A-I band striation pattern of the cells is made with either a Zeiss Achromat 40X (NA = 0.75) or a Plan Neofluar 63X (NA = 1.2) (Carl Zeiss, Inc.) water immersion DIC objective. The cell may be observed visually under bright-field or DIC illumination for initial set up and adjustment or projected through the trinocular phototube onto a 35-mm camera or 1,728 element charge-coupled device (CCD) photosensing array (Reticon Inc., Sunnyvale, CA). The 1,728 element self-scanning CCD optical sensor supplies sequential

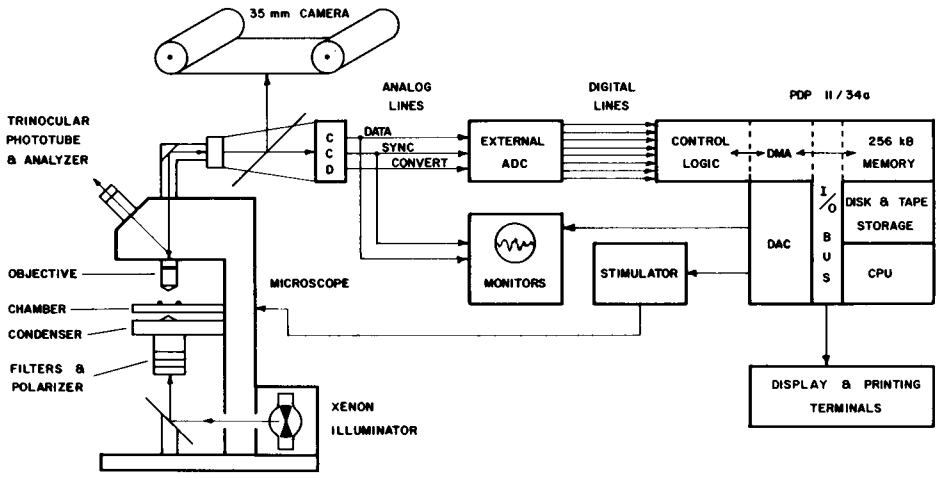

FIGURE 2 Direct image apparatus.

analog voltages linearly proportional to the striation pattern image intensities and the necessary synchronizing control pulses (convert and frame synchronization). These three signals are fed through a high-speed external analog-to-digital converter (ADC) direct memory access (DMA) data acquisition system interfaced with a PDP 11/34a computer (Lieber et al., in press, 1982). Eight-bit digital representations (256 levels) of the voltages from the CCD elements are sequentially stored into the 192K bytes of computer memory available for data storage every 1.43 μs (700 KHz) at full speed. Thus, up to 108 sequential 1,728 element frames of data may be collected at one time with a maximum full frame rate of ~2.5 ms/frame. Slower data rates were usually used (70–300 KHz) to allow sufficient time to cover a complete cardiac muscle contraction cycle and improve the system's signal-to-noise ratio.

Data Acquisition

Using this upgraded direct image apparatus, calibration grid or striation pattern images are obtained under computer control. An aliquot of isolated cells is placed in the microscope's imaging chamber. The cells are visually scanned under low power and a single cell is selected according to the previously described criteria. The cell and chamber (or calibration test grid) are rotated about the optical axis so as to align the long axis of the selected cell (perpendicular to its striation pattern) with the axis of the CCD array and the direction of shear of the DIC optics. This minimizes any geometrical alignment error (Roos et al., 1982) and provides for the maximum use of the contrast enhancement capabilities of the Normarski DIC system when used for striation pattern imaging (see Results and Discussion).

Direct-image data can be obtained under a variety of protocols with the flexible MACRO-11 computer acquisition program (Digital Equipment Corp., Maynard, MA). During an experiment, the image is constantly being scanned by the CCD detector and displayed on the oscilloscope monitor in real time at a rate determined by the detector's manually adjustable master clock (70–700 KHz). Depending on the desired experiment, the operator selects a specific set of data collection parameters: the number of frames of data to be saved (1–108); the number of data frames skipped between saved frames (0–99); and synchronized stimulus on/off. After a set of data is obtained, it is replayed on the monitor by the computer in slow motion to check for any obvious failure of experimental execution (i.e., lack of synchronization or stimulation, etc.) before permanent storage on magnetic disk or tape for formal analysis. In this way, single scans of image data are recorded from resting/quiescent isolated cells or multiple sequential scans are recorded from phasically contracting cells after stimulation. At maximum speed, the direct image system is capable of 2.5 ms frame rates (700 KHz) but is restricted to 6.0 ms (300 KHz) rates when the lower image intensity Nomarski DIC methodology is utilized. Frame rates of 13 ms (133 KHz) have been used in the sequential imaging mode and appear adequate to freeze dynamic sarcomere movement. During each experiment additional data are recorded from precision transmission gratings to calibrate the system magnification, and from uniformly lit background (no object) to reduce any systematic element by element CCD detector noise.

Data Analysis

Hill/valley intensity profiles of isolated cell striation patterns (Fig. 7) or calibration test grids (Fig. 5) stored on disk or tape are evaluated frame by frame with an interactive FORTRAN analysis program. The raw digitized video data consist of several components: (*a*) the striation pattern (or test grid) image signal; (*b*) a low-frequency modulation of light level due to the differential opacity of the isolated cell preparation (Roos et al., 1982); (*c*) fixed CCD element differential gain factors (±15%); and (*d*) random dark current CCD detector noise (±1 of 256 intensity units). The first component is the signal desired for analysis; the remaining raw signal components are eliminated or reduced using digital processing techniques.

First, the background (uniform light) signal obtained during the experiment at the same overall light level is subtracted from each frame of intensity profile data to correct any differential gain in the CCD elements. The random dark current noise is reduced by using multiple sweep acquisition to allow signal averaging of the background data (always) and the intensity profile data (when not dynamic). This procedure not only reduces the intensity profile data noise but also eliminates the possibility of increasing the noise through superposition during background subtraction. These two techniques substantially reduce the noise inherent in the CCD detector to less than one-half an intensity unit (Fig. 5). Finally, any residual high-frequency random noise and the low-frequency light level modulation (probably due to the differential opacity of mitochondria and nuclei within an isolated cell) are digitally band-pass filtered (Walraven, 1980). The level of nonrecursive filtering is small (the usual band-pass cutoffs are from 15 to 100 CCD element spacing units about the usual 30–40 element periodicity of the sarcomeres) and no extraneous nonlinearities or phase shifts are introduced in the process that might distort striation position. Direct comparison of filtered with unfiltered data (Fig. 7) demonstrates only a slight rounding of abrupt edges and a leveling of base-line irregularities that are due to differential regional opacity. After this digital image processing, the intensity profile has clearly defined hills and valleys under the low light level Nomarski DIC conditions (Fig. 7). The fully processed hill/valley intensity profiles are then analyzed to determine their centroid and peak (max/min) positions (Lubell and Roos, 1980).

There are a number of systematic errors that can effect the precision of

this striation position detection method and the resulting calculated sarcomere length. Given that the hill/valley intensity profile corresponds to the muscle's light/dark striation pattern (optical resolution is discussed in the following section), errors in calculated sarcomere lengths can be introduced by vertically or rotationally misaligned isolated cells, and by the discrete spatial CCD element by element nature of the data. These factors have been extensively quantified in a previous manuscript (Roos et al., 1982), and the magnitude of this error is the same as before (−1.5% to +3.0% about a 2.0 μm sample).

Though the total detection error remains the same as before, an additional effort has been made to insure that discrete centroid detection precision is better than ±1 CCD element or ±0.05 μm at the usual 300X magnification factor. The CCD sensor mounting to the microscope was modified to incorporate a translating micrometer between the two. The sensor can be precisely moved along its long axis relative to the magnified microscope image in steps as short as 0.033 μm (a 10 μm micrometer step/300X magnification factor). This is far more accurate than moving the specimen relative to the microscope's objective under stage control. Several gratings and quiescent isolated cells have been examined while sequentially translating the sensor across their image in a series of steps of various magnitudes. Fig. 3 illustrates a sample of three striations from an isolated cell tracked through a series of 15 translation steps over an equivalent object distance of 1.0 μm. The detected position for each striation position is within ±1 CCD element spacing (±0.05 μm) of the translated micrometer position. This produces the relatively linear response observed. The discrete steps occur because most of the translated steps are less than the adjacent CCD spacing. This clearly demonstrates the accuracy of this centroid detection method in determining small changes striation position and thus sarcomere length.

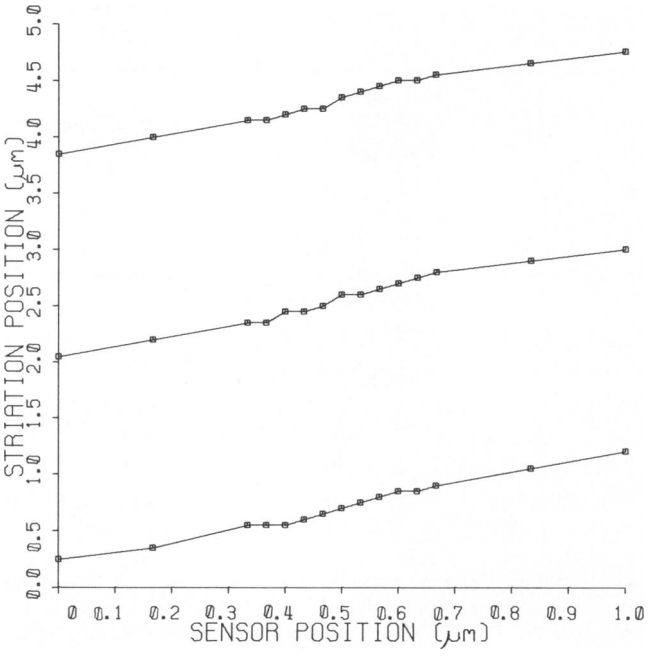

FIGURE 3 Striation position sensitivity. Three striations are tracked through 15 translation steps of the sensor relative to the fixed cell image. The abscissa is the position of the CCD sensor as controlled by a translating micrometer in calibrated μm units. The ordinate is in detected hill centroid position in calibrated μm units.

RESULTS

Striation Resolution (Test Grid)

Concepts of Optical System Resolution. The direct image apparatus (Fig. 2) translates the striation pattern profile from an isolated cell (Fig. 1) or calibrated test grid (Fig. 4) into an intensity profile of hills and valleys (Fig. 5 and 7). In a positive contrast image, the hills would represent the variable width I bands and the valleys the 1.5-μm wide A bands from the sampled cell image volume (63X objective, 300X system magnification) of 86 μm long, 0.053 μm wide, and 0.23 μm deep. The intensity profile from a negative contrast image (as commonly used with Nomarski, DIC) merely inverts this configuration leaving the basic optical principles unchanged. The following discussion will assume negative contrast images for heart cells and positive contrast for test grids.

If one could produce a perfect image of the striation pattern of an isolated cell with monochromatic light and infinite resolution optics, one would expect the intensity profile to resemble a square-wavelike densitometer trace from an electron micrograph. Unfortunately, even the best light microscope optical systems are diffraction limited (i.e., images are broadened by the wavelength-dependent bending of light at geometrical edges) and suffer to some extent from spherical and other nonlinear optical abberations (Born and Wolf, 1964; Martin, 1966; Smith, 1966). Thus, the more rounded sinewavelike intensity profiles are observed from both test grids and isolated cell striation patterns (Fig. 5 and 7).

These real optical system considerations have led to the use of standard criteria for resolving power of light microscopic optical systems. One widely used measure, Sparrow's criterion (a corollary of the Rayleigh criterion), requires an image separation such that the maximum of one line falls on the first minimum of an adjacent line (Smith, 1966). A real optical system such as the one used in our direct-image system with a polychromatic Xenon light source can be treated as an incoherently illuminated system (personal communication, Carl Zeiss, Inc., New York). Then, in the case of a slit aperture (similar to a muscle striation), the diffraction limited resolving power Y with incoherent illumination would be determined by the following equation

$$Y = \frac{0.50\lambda}{NA} \quad (1)$$

where λ is the wavelength of light and NA is the numerical aperature of the optical system. From this equation, the expected resolution of our 63X, 1.2 NA objective would be 0.23 μ and of our 40X, 0.75 NA objective would be 0.37 μm, assuming an average 0.55 μm wavelength of light (Table I).

Muscle striation pattern periodicity exceeds these values by at least four to sixfold, but I band widths could be much less during a contraction. That does not mean that I bands cannot be visualized at sarcomere lengths shorter than 1.73 μm with the 63X objective, because it is the relative amount of detectable contrast between the A and I band

TABLE I
OPTICAL SYSTEM PERFORMANCE

Objective	Numerical aperture	Optical condition	Theoretical image spread	Observed image spread	Effective numerical aperture	Contrast at 0.05 μm
			(μm)	*(μm)*		*percent*
40X	0.75	bright-field	0.37	0.79	0.35	5
63X	1.20	bright-field	0.23	0.43	0.64	10
63X	1.20	Nomarski DIC	0.23	0.28	0.98	15

images (ΔI) that is critical (Inoué, 1981). For example, an opaque bar of the standard criterion width (0.23 μm for the 63X objective) on a luminous background would produce an image intensity drop of 78%; that is, the luminous background level equals 1.00 and the opaque bar equals 0, the opaque bar image would have a relative observed intensity of 0.22 (Martin, 1966). However, as little as 3% changes in intensity between parallel lines might be visually appreciable (Martin, 1966). Furthermore, linearly responding detector systems such as our CCD (or the TV detectors of Rieser et al., 1979; Allen et al., 1981 *a* and *b*; Inoué, 1981; Walter and Berns, 1981) can exceed the contrast performance of the nonlinear human eye or photographic film especially when coupled with optical contrast enhancement techniques (phase-contrast or DIC) and computer digital image processing. Thus, the conventional criteria for image resolution do not necessarily apply and are somewhat arbitrary. The actual resolving power for an optical image detector system such as the one used for these studies must be determined empirically.

Evaluation of Direct Image Optical System. By way of evaluating the Zeiss optical system used in conjunction with our direct image apparatus, a specially designed modulation transfer-function test grid was critically examined with both immersion objectives. This coated glass grid consists of 10 ~1-μm wide clear lines etched with an electron beam at a 2.0 μm period (exact) followed directly by 10 more 1-μm wide clear lines etched at a 3.0 μm period. Figs. 4 *a* and *b* are 63X objective photomicrographs of this

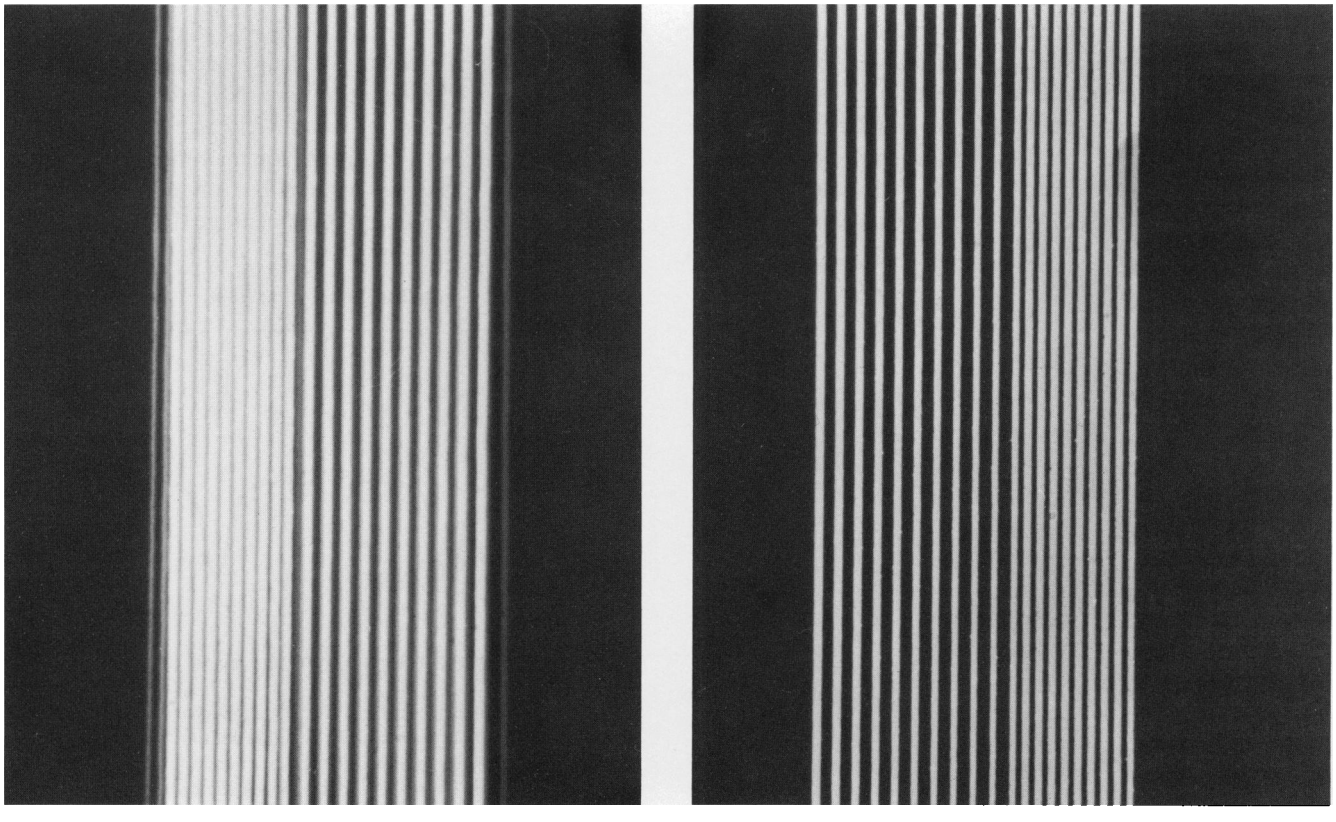

FIGURE 4 Photomicrographs of test grid. A 2.0-3.0 μm period test grid is imaged with the 63X objective and photographed under standard bright-field microscopy with (*a*) stopped down condenser and (*b*) matched condenser-objective. Full NA conditions.

grid under (*a*) a stopped down (reduced effective NA) condenser and (*b*) matched condenser-objective—full NA conditions. Compare the clarity of the matched condenser image of Fig. 4*b* to the relatively fuzzy and multiple-lined image of Fig. 4 *a*. It is often necessary to stop down and reduce the condenser aperture diameter under standard bright-field illumination conditions to see any detail in unstained biological specimens such as isolated cardiac cells. This apparent increase in detail is obtained with an accompanying loss of resolution due to the lowering of the microscope's effective numerical aperture which gives the observed fuzzy image of Fig. 4 *a*. Conversely, matched condenser-objective high numerical aperture bright-field images of unstained biological specimens usually appear unclear and washed out with stray light, but in reality they are of maximum resolution and can be imaged clearly with linear TV or CCD detectors (Allen et al., 1981 *a* and *b*; Inoué, 1981). Matched condenser-objective conditions are also used with Nomarski DIC contrast enhanced images (Allen et al., 1969).

Fig. 5 is the central portion of the unfiltered intensity profile of this test grid near its 2–3 μm period transition zone imaged with the 63X, 1.2 NA objective and matched condenser under DIC conditions. This figure clearly demonstrates the sharp and virtually complete (for 3.0 μm period) transition from clear to opaque zones in this known test object. By counting the number of calibrated detector elements along the 3 μm period light-dark transitions and at a single light-dark edge, the real image spread about a true geometrical edge was determined for both objectives under the conditions actually used for isolated cell striation pattern recording (Table I). For the 63X objective, the observed image spread was 0.28 μm with Nomarski DIC and 0.43 μm under standard bright-field conditions; the 40X objective demonstrated a bright-field image spread of 0.79 μm. As expected, the observed spread values are about twofold greater than the theoretically derived numbers due to the real optical system abberations and polychromatic illumination (Smith, 1966). The Nomarski DIC image has substantially less spread illustrating its edge enhancement characteristics (Allen et al., 1969). The effective numerical apertures are also calculated from each spread value using Eq. 1 for each optical condition in Table I.

This test grid is obviously not an isolated cardiac cell, but it can provide a known basis of optical system performance from which to interpret striation pattern intensity profiles. For example, Fig. 6 illustrates the reconstructed image that would be recorded with the direct image system from an irregular geometrical pattern. This geometrical pattern is generally representative of a negative contrast striation pattern image of a grossly nonuniform isolated cell, though a real optically imaged A-I band interface is probably nowhere near as sharp (see later discussion). As seen in this schematized reconstruction, the images of each 1.5-μm wide clear zone (similar to an A band region) can be considered independently (---) with an assumed image spread of 0.40 μ about each geometrical edge. The images of adjacent 1.5 μ clear zones overlap in the variable width opaque zones (similar to I band regions). Their summation results in the observed reconstructed optical image (—), and the apparent valley intensity is proportional to the amount of overlap. In other words, the narrower the opaque zone, the greater the image overlap and the less apparent the hill/valley contrast. Nonetheless, even an 0.05-μm wide opaque zone would yield an easily detectable 11% drop in intensity relative to the maximum level in this example. For a narrow opaque bar on luminous background (or the converse), the percentage drop in intensity

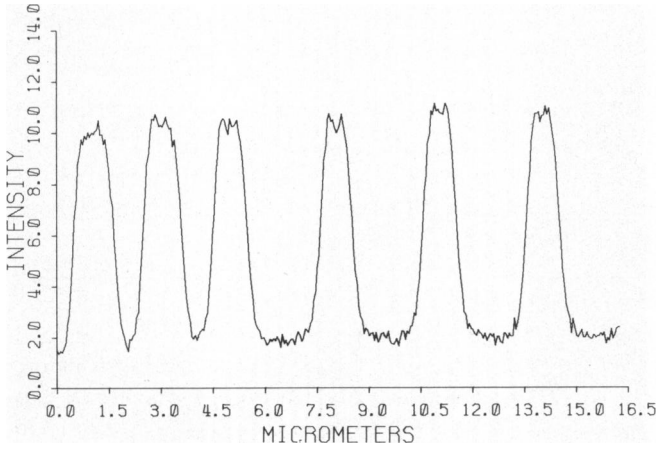

FIGURE 5 Intensity profile of test grid. The 63X Nomarski-DIC image intensity profile from the 2.0-3.0 μm transition zone of the calibrated test grid is plotted. The data has been CCD element gain corrected by background subtraction but has not been band-pass filtered. The abscissa is the calibrated length in μm along the sensor and the ordinate is the intensity of light at each element in arbitrary units.

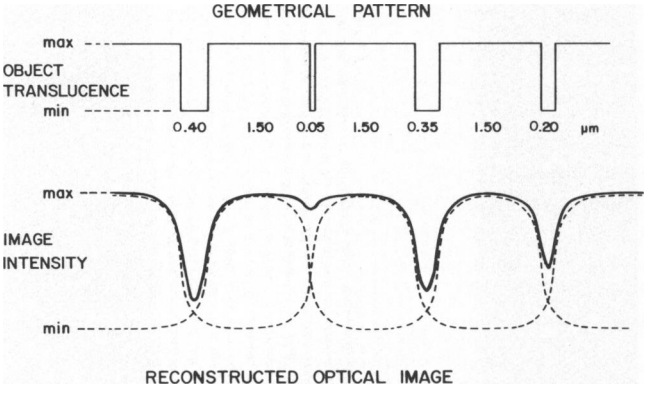

FIGURE 6 A geometrical pattern (top) has been constructed with 1.5-μm wide translucent zones separated by variable width (0.40, 0.05, 0.35, and 0.20 μm) opaque zones to represent a grossly nonuniform muscle striation pattern. An optical image has been reconstructed (bottom) from the geometrical pattern assuming a 0.40 μm image spread about each side of the geometrical edges. The image from each translucent zone is shown with dashed lines (---). The observed image (—) is the summation of each superimposed dashed-line image.

relative to background (or contrast C) can be calculated by the following equation:

$$C = \frac{\Delta I}{I_{max} - I_{min}} = \frac{16\,\delta\,NA}{3\pi\lambda} \quad (2)$$

where δ is the width of the bar (Martin, 1966). For $\delta = 0.05$ μm (minimum CCD detector resolution) and $\lambda = 0.55$ μm, the contrast for our optical system is

$$C = 0.154\,NA \quad (3)$$

where in this case NA is the effective numerical aperture for each imaging condition (Table I). Even the 5% relative intensity change of the 40X objective is easily detectable because the fully processed intensity profile signal-to-noise ratio exceeds 20:1 under matched objective/condenser bright-field conditions. Thus, narrow regions of differential translucency on the order of 0.05 μm from contracting muscle can be detected within the precision of the CCD pixel spacing.

Another issue of great concern is illustrated in this idealized reconstructed image diagram (Fig. 6). Because there is a finite spread to any image at a geometrical edge, there is some image overlap when the geometrical edges are sufficiently close together. This could lead to an erroneous detection of centroid positions if there is gross nonuniformity (as in Fig. 6). In this geometrical example, the problem is due to the slight shift in calculated centroid position of a hill away from its true position toward the narrower valley due to the inclusion of small portions of each adjacent image within the analyzed area. For example, the first hill (—) in Fig. 6 is located between two valleys caused by the less intense geometrical regions of 0.40 μm and 0.05 μm in width. The hill centroid is calculated from the minimum of one valley to the minimum of the next. Because the image from adjacent hills overlaps unequally on each side of this hill, there is an erroneous shift in the centroid of this hill. In this example, the 0.05 μm separation contributes 3.33% of the adjacent hill's image intensity (---) within the region of centroid calculation; the 0.40 μm separation contributes 1.45% on its side. Thus, there is a 1.88% shift in the hill image profile (—) to the right from the true centroid of that 1.5 μm wide aperture, if it was isolated (---). Because the actual spacing between the valleys in this case is 1.725 μm and would cover 34.5 CCD elements at the usual magnification factor, this 1.88% shift would represent <1 CCD element (2.9% of the distance/element). In a perfectly uniform muscle, the image overlap is symmetrical and there is no net detected centroid shift. Finally, it should be noted that the centroid positions of all the valleys (in the negative contrast condition) are always true in this schematized muscle diagram since they are separated by constant A band width at least 4 times the image spread value and thus have no adjacent valley image interdependence. All the above considerations apply when the contrast is inverted.

DIC Contrast Enhancement. As noted in Table I, the utilization of Nomarski DIC methodology substantially increases the effective numerical aperture and test-grid image sharpness. Isolated cardiac cells have the typical shadow cast appearance of DIC microscopy (Fig. 1). When properly adjusted, the Zeiss-Nomarski DIC system used in these studies crisply shows the striation pattern of the cells with high-contrast. This Zeiss system utilizes polarizers and Wollaston prisms above and below the object (similar to other commercially available DIC systems) to produce a high extinction shear inteference phenomenon (Lang, 1968 and 1969*a*; Allen et al., 1969 and 1981*b*). The crossed polarization provides the high extinction (up to ~1,000-fold decrease in nonbirefringent object intensity), low glare image that permits the visualization of high contrast at large numerical apertures. It is this glare from scattered light that washes out visual images (such as muscle striation patterns) with standard bright-field microscopy at large numerical-aperture matched objective-condenser conditions. The Wollaston prism arangement in the Zeiss DIC system produces a small shear (a beam separation near the magnitude of the objective's theoretical diffraction limitation) in the object plane (Allen et al., 1969). The image intensity obtained from this type of small shear DIC system is primarily dependent on the phase gradients within the object. In striated muscle where there is a phase gradient at the A-I band interface, there is a relatively large change in DIC contrast. Thus when the muscle's striations are oriented perpendicular to the direction of shear and when the bias compensation (alignment of beam separating and reforming prisms) of the Wollaston prisms is adjusted near maximum extinction and zero phase shift, a high-resolution, high-contrast visual image of the striation pattern is obtained.

When recording images with relatively linear external detectors (TV or CCD), instead of direct human eye observation, the proper selection and adjustment of the optical components of a polarization based microscope system (such as DIC) can provide greatly enhanced contrast at maximum resolution (Allen et al., 1981 *a* and *b*; Inoué, 1981). Inoué (1961, 1981) has developed an elegant polarizing microscope using his own specially designed rectification optics that provide a very high-extinction, low-glare image. This results in a very high-contrast but low-intensity image well suited to his video detector. On the other hand, Allen (1981*b*) obtains high-contrast images with conventional optical components coupled to a video camera by adjusting the bias compensation away from the normally nearly aligned settings to relatively large values of phase retardation ($\lambda/9$–$\lambda/4$). These images appear visually washed out by stray light, much like the

previously discussed matched condenser-objective bright-field conditions. But as illustrated in his Fig. 6 (Allen et al., 1981*b*), the contrast available at these relatively low extinction settings is actually greater (if detectable) than that obtainable at the usual high extinction settings which are necessary for visual observation without losing the beneficial high-resolution characteristics of DIC. In fact, Allen et al. (1981*b*) claim that the greatly increased bias retardation further reduces any stray rotation or phase shifts from specimen features above or below the plane of focus. Both Inoué's (1981) and Allen et al.'s (1981 *a* and *b*) systems have clearly detected specimen features on the order of 50–100 nm.

Because one of the goals of this study on isolated cardiac cells is to follow the striation pattern during a dynamic phasic contraction, the use of 33 ms fixed-frame-rate TV-based detectors was precluded. It was necessary to build our direct striation-pattern detection system around solid-state CCD technology. The drawbacks to this approach are that CCD are not as light sensitive as some TV detectors, their output is inversely proportional to frame rate, and they have differential element by element gain factors. These deficiencies are substantially reduced by the previously outlined use of high intensity illumination and computer image processing. Furthermore, CCD detectors can be run at considerably faster frame rates than standard TV systems, are lag free (no image retention), and respond linearly over a 500:1 dynamic range (Roos et al., 1980). It is not possible to use ultra-high extinction techniques such as did Inoué (1961, 1981) with our direct image system because there would be insufficient light intensity for CCD operation. Instead, we adjust the Wollaston prism of our Zeiss DIC system for maximum contrast with our CCD. This low extinction–high bias compensation approach (similar to Allen et al., 1981*b*) provides adequate light intensity for the CCD, crisply defined DIC enhanced striation patterns, and minimal stray rotation and phase effects from nonfocused material in the specimen. There is sufficient light intensity to utilize the optional DIC methodology in the direct-image system for dynamic striation pattern data acquisition at rates up to ~300 KHz (6 ms/frame) with the 63X objective. Thus, the utilization of highly bias-compensated DIC (such as the commercially available Zeiss-Nomarski type incorporated into the direct image apparatus) can provide improved resolution and high contrast images of isolated cell striation patterns when coupled to external detectors and digital computers.

Striation Resolution (Single Heart Cell)

Correlation of Optical System Performance to Muscle Images. In translating these empirically based theoretical optical system observations into terms comparable to real striation patterns from isolated cardiac cells, it appears that there is little centroid detection distortion unless there is gross nonuniformity of sarcomere lengths and the A-I band junction is optically very diffuse. It is unlikely that the A-I band junction in the muscle is as sharp as the idealized geometrical edges of Fig. 6. In fact, a somewhat diffuse A-I band junctional region would tend to round off the observed striation pattern profile to the more sinusoidal shape seen in both the filtered and unfiltered intensity profile in Fig. 7. Increasing the amount of high-frequency filtering by reducing the filter bandwidth would further round off the pattern. But levels of filtering greater than that illustrated in Fig. 7 are not used and are unnecessary for analysis. Nonetheless, a softened A-I band interface would not appreciably affect our determination of the striation pattern centroid position. This is a reasonable assumption because any misalignment or skewing of the thick filaments is probably random, symmetrical, and in any case averaged out within a given focused myofibrillar area. Furthermore, there appears to be little interference from phasic material, mitochondria, and nuclei above and below the focal plane especially when Nomarski DIC methodology is used. Under these conditions it is possible to selectively focus within these 15–20 μm thick isolated cells in such a way that nuclei are sharply in focus at one setting and are completely replaced by striation pattern just a few microns above or below. Allen et al. (1969) have noted that the depth of image influence is ± 3 Airy radii above or below the plane of focus with Normarski DIC at the normal high extinction adjustment. For our system, that would translate to ~1.6 μm (no greater than two myofibril diameters) and in reality may be better when high bias compensation is used (Allen et al., 1981*b*). Though not free from some uncertainty, there is sufficient evidence that the intensity profile of the striation pattern from isolated cardiac cells provides a reasonably accurate representation of discrete sarcomere periodicity.

Dynamic Striation Pattern Recording. Intensity profiles from isolated cardiac cells demonstrate the clearly defined A-I band striation patterns (Fig. 7). This example is a portion of a partially and fully computer processed 63X Nomarski/DIC enhanced image from a resting cell. This hill and valley intensity profile is a reasonably good representation of the A and I band striations within the projected image volume of the cell, subject to the limitations of the direct image system and actual microstructure of the muscle as previously discussed.

To illustrate the dynamic cell image recording capabilities of the direct-image system, sequential intensity profiles have been acquired from six electrically paced phasic contracting cells at a 133 KHz - 13 ms frame rate under 40X objective bright-field conditions. After initial individual frame computer processing to determine hill and valley centroid position, each striation may be selectively tracked

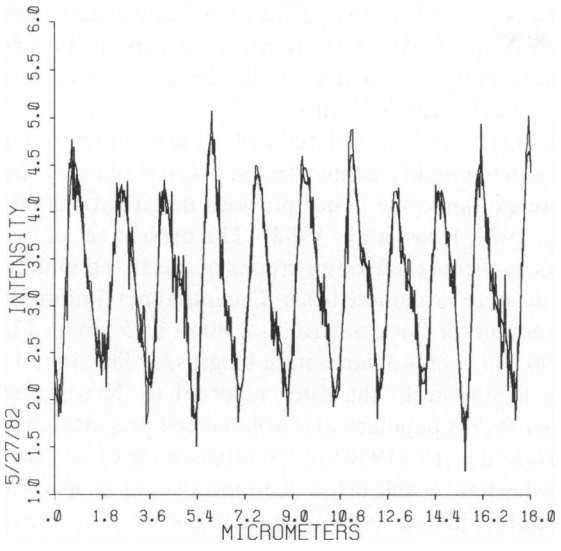

FIGURE 7 Isolated cell intensity profile. A portion of partially and fully computer processed hill and valley 63X DIC intensity profile of an isolated cardiac cell is plotted. The more abrupt and jagged line represents a 400 CCD element portion of a signal averaged, background subtracted, and high pass digitally filtered (cutoff = 15 elements) intensity profile. The superimposed, smoother line is the same data after low-pass filtering (cutoff = 100 elements). The abscissa is the calibrated length in micrometers along the sensor, and the ordinate is the intensity of light at each element in arbitrary units.

by the computer through the entire dynamic data set to produce a striation position vs. time map (Fig. 8). In this example, eight adjacent hill and valley centroid-determined striation positions are plotted through the 60-frame contraction-relaxation cycle of this isolated cell. The striation positions translate relative to the fixed sensor element position because each end of the cell shortens relative to the center. The translation of each striation is smooth with no evidence of erroneous centroid tracking or stepwise shortening (it is not likely that a 13 ms frame is sufficiently fast to detect this later reported phenomenon in cardiac muscle, [Pollack et al., 1977]). The hill and valley centroid positions in this example are not perfectly symmetrical. The exact source of the asymmetry in Fig. 8 is not known, but the same effect can be controllably induced on the CCD recorded intensity profile by miscentering the condenser under bright-field conditions. Fortunately, an asymmetry of this type is very consistent from striation to striation along the length of the cell and throughout the dynamic cycle. There is no effect upon sarcomere length determination because it is derived from calibrated hill to hill or valley to valley spacing.

The sarcomere length, as determined by the calibrated spacing between adjacent hills or valleys in Fig. 8 first decreases, then increases during the contraction-relaxation cycle. This relationship is replotted in Fig. 9 for the average sarcomere length (the smoothly changing line) and two sample sarcomeres (the discretely changing lines) from nonadjacent sarcomeres. The shape of the individual sarcomere length vs. time plots is qualitatively similar to the average for all the samples no matter where they are located within the cell. Some sarcomeres are consistently longer or shorter than the average throughout the cycle. The discrete steps of the individually tracked sarcomeres

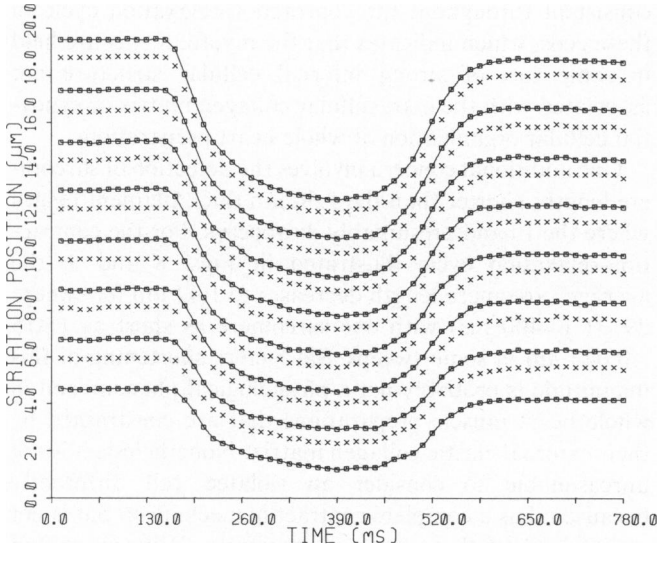

FIGURE 8 Dynamic striation map. Eight hill (□) and seven valley (×) centroid positions are tracked through a complete phasic contraction-relaxation cycle of an isolated cardiac cell. Only the hill centroid positions are connected by lines for ease of differentiation. The abscissa is the time in millisceonds during the image sampling period, and the ordinate the centroid postions of each striation in micrometers. 40X objective bright-field conditions.

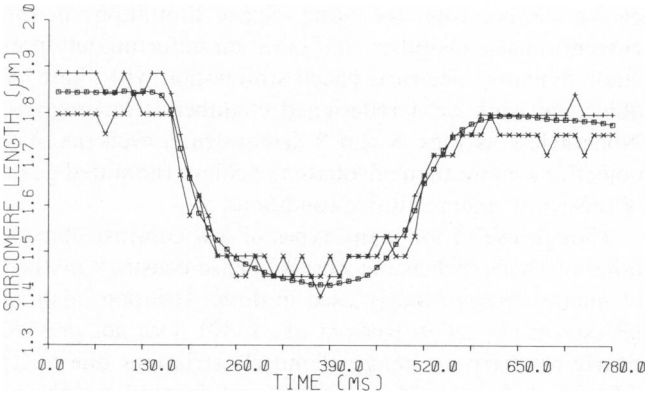

FIGURE 9 Average and individual sarcomere length tracking. The change in average (□) and in two individual sarcomere lengths (Nos.7[+] and 15[×]) are plotted together from the same contraction relaxation cycle in Fig. 8. The discrete vertical steps in sarcomere length reflect the ±1 CCD element detection precision of the system. The abscissa is the time in milliseconds during the image sampling period and the ordinate the calibrated sarcomere lengths in micrometers.

reflect the ±1 CCD element (or ±0.044 μm in this case) precision of the detection system.

DISCUSSION

It is one of the goals of this study to critically evaluate the isolated heart cell direct imaging system to quantify its maximum striation pattern detection characteristics and its limitations. Traditional light microscope resolution criteria are generally based on human eye evaluation (Martin, 1966; Smith, 1966). Though no optical system can perfectly image object detail, it has been shown that relative to the human eye, higher resolution images than previously thought possible can be detected by carefully selecting, matching, and adjusting optical components and detector systems (Allen et al., 1981 *a* and *b*; Inoué, 1981; Walter and Burns, 1981). We have carefully evaluated the image performance characteristics of our computer-coupled CCD detected direct-image system with known test and calibration grids and found it sufficient for its designed purpose of dynamically imaging heart cell striation patterns. The empirically derived optical performance characteristics of our system (Table I) are quite reasonable considering the state of the art optics, electronic hardware, and computer software used. There is sufficient resolution and contrast capability in the direct-image system with either objective to detect muscle striation patterns throughout a contraction-relaxation cycle along the length of an intact isolated cardiac cell. Small changes in striation position and therefore sarcomere length are reliably quantified within the ±1 CCD element spacing limits empirically evaluated.

The incorporation of Nomarski DIC improves the optical performance characteristics of the direct-image system under high bias-compensated matched condenser conditions (Table I). Given sufficient light intensity, the 63X objective with DIC is the optical combination of choice for precision recording. Space limitations in the current muscle chamber configuration unfortunately preclude dynamic electrical paced stimulation with the 63X objective; work on a redesigned chamber is in progress. Nonetheless as Figs. 8 and 9 demonstrate, even the 40X objective is more than adequate to achieve the stated goals of this study under suitable conditions.

Though useful for many types of low contrast objects, other methods such as the Zernike phase-constrast method of microscopy previously used in direct striation imaging (Rieser et al., 1979; Roos et al., 1982) does not provide nearly as sharp an image of muscle striations due to its inherent halation (edge-ringing) and focal-plane phase-reversed phenomenon (Lang, 1969 *b*). Walter and Burns (1981), however, have been able to substantially improve video-detected phase-contrast images with on-line computer signal processing techniques. Their differential phase-contrast system image quality approaches, and in some cases exceeds, standard DIC image quality. On the other hand, the interference microscope designed and built by Huxley (1954, 1958) for his early muscle studies works on the same basic interference principles as the Zeiss-Nomarski DIC system except that the lateral beam separation is much larger (74 μm).

The Ca^{2+}-tolerant isolated cell, as used in these experiments, has visually demonstrated a rapid phasic contraction-relaxation cycle in our previous investigations (Brady et al., 1979; Roos et al., 1982). The present set of experiments confirms these observations of speed and uniformity on a discrete sarcomere basis. The initial maximum rate of contraction for this cell (from ~1.80 to 1.55 μm, in Fig. 9) is 4.90 μm/s or ~3 sarcomere lengths/s. This initial rate value is similar to the rates reported by Krueger et al. (1980) for rat papillary and isolated cell preparations. But unlike Krueger's (1980) observations most of our isolated cells shorten to well below 1.50 μm during an electrically stimulated phasic contraction. The rate of contraction below 1.55 down to 1.43 μm in this example is a considerably slower 1.0 μm/s. This slower contraction rate could be due to either thick filament–Z band interference at short sarcomere lengths or to some as yet undefined reduction in contractile activation. Relaxation occurs nearly as rapidly as contraction (3.85 μm/s from 1.50 to 1.65 μm). The entire average sarcomere length–time relationship is qualitatively similar to that of Krueger et al. (1980); however, we do not observe any gross change in sarcomere uniformity throughout the cycle. The standard deviation of sarcomere lengths in each sweep of this 60-sweep sample ranged randomly from ±0.036 μm to ±0.075 μm with a grand mean of ±0.053 μm. As determined from discrete striation positions, sarcomere length uniformity is quite consistent throughout the contraction-relaxation cycle in these cells, which indicates that the myofilaments are held in some sort of strong internal cellular structure not associated with the extracellular collagen matrix or syncytial cellular organization of whole heart preparations.

One additional concern involves the detection of sarcomere lengths shorter than the 1.50 μm thick filament length where the I band presumably disappears. For the contraction-relaxation cycle illustrated in Figs. 8 and 9, the average sarcomere length decreases to 1.42 μm for sweeps 29–31 (~400 ms) with one sarcomere as short as 1.315 ±0.044 μm in some sweeps. Sarcomere shortening of this magnitude is probably not a physiological phenomenon in whole heart muscle preparations that are constrained by their external elastic collagen matrix. Nonetheless, it is not unreasonable to consider an isolated cell differently because it has a complete contractile mechanism but is not constrained by these external structures. Wittenberg and Robinson (1981) have shown an electron micrograph of a phasically contracted isolated cell (their Fig. 4) that indicates a residual I band region (including Z disks) of 12–15% of the total 1.50 μm (1.40 μm as measured by these investigators) sarcomere length or ~0.20 μm. In fact, if this observation is valid, it indicates that there is an adequate differential refractive index with the adjacent

A-band material to facilitate optical striation pattern recording at short sarcomere lengths. Our data indicate that there is no greater than a 50% drop in hill-to-valley maxima (contrast) from resting to fully contracted intensity profiles, which would imply a similar optically observable A band separation of 0.20 μm (Fig. 6). The continuously tracked hill and valley striation positions plotted in Fig. 8 also indicate no light-dark phase reversal of the image as might be expected during contraction band formation due to overlapping thick filaments. Krueger and London (1982) have more critically examined the optically observable striation patterns from isolated heart cells at short sarcomere lengths with Jamen-Lebendeff interference microscope system and matched refractive index bathing solutions. They also observed no phase reversal or contraction band formation in electrically paced phasically contracted intact isolated cells as short as 1.40 μm. However, they do observe these phenomena in chemically skinned or barium-treated cells. This evidence suggests that at least in intact cardiac cells unconstrained by any external elastic matrix, there is some internal structural component that inhibits the expected contraction band formation. Whatever its source, this preservation of the striation pattern at short sarcomere lengths appears to be a real phenomenon and provides the means from which discrete sarcomere lengths can be tracked throughout a complete phasic contraction-relaxation cycle.

This manuscript has detailed the development and implementation of a high-speed, high-resolution direct optical imaging system specifically designed to determine discrete sarcomere lengths in isolated cardiac cells. The optical performance of this imaging system has been determined and applied to real muscle striation pattern conditions. Discrete striations from isolated rat cardiac cells can be detected and followed during electrically paced contraction-relaxation cycles with high accuracy. Individual sarcomeres appear to contract and relax in unison though there is a nonuniformity of sarcomere lengths. Their maximum rates of contraction and relaxation indicate the contractile and excitation control mechanism is intact and fully functional. This type of Ca^{2+}-tolerant isolated cell preparation directly monitored by the on-line direct-imaging system shows much promise for the study of cardiac muscle performance with a well-defined experimental system.

We are grateful for the many helpful discussions on optical microscopy with Dr. Alfred F. Leung. Additionally, we thank Bradford A. Lubell, Laurie Kafesjian, and Ted Tan for their technical assistance in the software development, data analysis, and cell preparation for the experiments reported in this manuscript.

This work was supported in part by National Insitutes of Health Grant HL 11351-15 to Dr. Brady, and American Heart Association, Greater Los Angeles Affiliate, Equipment and Grants-in-Aid to Dr. Roos.

Received for publication 20 May 1982 and in revised form 23 July 1982.

REFERENCES

Allen, R. D., G. B. David, and G. Nomarski. 1969. The Zeiss-Nomarski differential interference equipment for transmitted-light microscopy. *Z. Wiss. Mikrosk. Mikrosk. Tech.* 69:193–221.

Allen, R. D., J. L. Travis, N. S. Allen, and H. Yilmaz. 1981 *a*. Video-enhanced contrast polarization (AVEC-POL) microscopy: A new method applied to the detection of birefringence in the motile reticulopodial network of Allogromia laticollaris. *Cell Motil.* 1:275–289.

Allen, R. D., N. S. Allen, and J. L. Travis. 1981 *b*. Video-enhanced contrast, differential interference contrast (AVEC-DIC) microscopy: A new method capable of analyzing microtubule-related motility in the Reticulopodial network of Allogromia laticollaris. *Cell Motil.*. 1:291–302.

Born, M., and E. Wolf. 1964. Elements of the theory of diffraction. *In* Principles of Optics. Pergamon Press, Inc., New York. 370–458.

Brady, A. J., S. T. Tan, and N. V. Ricchiuti. 1979. Contractile force measured in unskinned adult rat heart fibers. *Nature* (*Lond.*). 282:728–729.

Cleworth, D. R., and K. A. P. Edman. 1972. Changes in sarcomere length during isometric tension development in frog skeletal muscle. *J. Physiol.* (*Lond.*). 227:1–17.

DeClerck, N. M., V. A. Claes, E. R. Van Ocken, and D. L. Brutsaert. 1981. Sarcomere distribution patterns in single cardiac cells. *Biophys. J.* 35:237–242.

Fabiato, A., and F. Fabiato. 1976. Techniques of skinned cardiac cells, and of isolated cardiac fibers with disrupted sarcolemma with reference to the effects of catecholamines and of caffeine. *Recent Adv. Stud. Card. Struct. Metab.* 9:71–94.

Fabiato, A. 1981. Myoplasmic free calcium concentration reached during the twitch of an intact calcium-induced release of calcium from the sarcoplasmic reticulum of a skinned cardiac cell from the adult rat or rabbit ventricle. *J. Gen. Physiol.* 78:457–497.

Ford, L. E., A. F. Huxley, and R. M. Simmons. 1977. Tension responses to sudden length change in stimulated frog muscle fibres near slack length. *J. Physiol.* (*Lond.*). 269:441–515.

Gordon, A. M., A. F. Huxley, and F. J. Julian. 1966. The variation in isometric tension with sarcomere length in vertebrate muscle fibres. *J. Physiol.* (*Lond.*). 184:170–192.

Huxley, A. F., and R. Niedergerke. 1954. Structural changes in muscle during contraction. Inference microscopy of living muscle fibres. *Nature* (*Lond.*). 173:971–973.

Huxley, A. F. 1957. Muscle structure, and theories of contraction. *Prog. Biophys.* 7:255–318.

Huxley, A. F., and R. Niedergerke. 1958. Measurement of the striations of isolated muscle fibers with the interference microscope. *J. Physiol.* (*Lond.*). 144:403–425.

Huxley, H. E., and J. Hanson. 1954. Changes in the cross-striations of muscle during contraction, and stretch, and their structural interpretation. *Nature* (*Lond.*). 173:973–976.

Inoué, S. 1961. Polarizing microscope: design for maximum sensitivity. *In* Encyclopedia of Microscopy. G. L. Clarke, editor. Reinhold Publishing Corp., New York. 480–485.

Inoué, S. 1981. Video image processing greatly enhances contrast, quality, and speed in polarization based microscopy. *J. Cell Biol.* 89:346–356.

Krueger, J. W., and G. H. Pollack. 1975. Myocardial sarcomere dynamics during isometric contraction. *J. Physiol.* (*Lond.*). 251:627–643.

Krueger, J. W., D. Forletti, and B. A. Wittenberg. 1980. Uniform sarcomere shortening behavior in isolated cardiac muscle cells. *J. Gen. Physiol.* 76:587–607.

Krueger, J. W., and B. London. 1982. Contraction band behavior in intact & chemically skinned, isolated cardiac muscle cells. *Biophys. J.* (*Abstr.*). 37:356 *a*.

Lang, W. 1968. Nomarski differential interference-contrast microscopy. *Zeiss Inf.* 70:113–120.

Lang, W. 1969 *a*. Nomarski differential interference contrast microscopy. II. Formation of the interference image. *Zeiss Inf.* 71:12–16.

Lang, W. 1969 *b*. Nomarski differential interference-contrast microscopy. III. Comparison with phase-contrast method. *Zeiss Reprint.* S 41-210.4.

Leung, A. F. Laser diffraction of single intact cardiac muscle cells at rest. *J. Muscle Res. Cell Motil.* In press.

Lieber, R. L., K. P. Roos, B. A. Lubell, J. W. Cline, and R. J. Baskin. High speed digital data acquisition of sarcomere length from isolated skeletal, and cardiac muscle cells. IEEE (Inst. Electr. Electron. Eng.) *Trans. Biomed. Eng.* In press.

Lubell, B. A., and K. P. Roos. 1980. A study utilizing RT-11, and an optical CCD device for sarcomere measurement in single cardiac cells. *Proc. Digital Equip. Comp. Users Soc.* 6:1243–1248.

Martin, L. C. 1966. The Theory of the Microscope. Am. Elsevier New York. 1–488.

Paolini, P., K. P. Roos, and R. J. Baskin. 1977. Light diffraction studies of sarcomere dynamics in single skeletal muscle fibers. *Biophys. J.* 20:221–232.

Pollack, G. H., T. Iwazumi, H. E. D. J. ter Keurs, and E. F. Shibata. 1977. Sarcomere shortening in striated muscle occurs in a stepwise fashion. *Nature* (*Lond.*). 268:757–759.

Powell, T., D. A. Terrar, and V. W. Twist. 1980. Electrical properties of individual cells isolated from adult rat ventricular myocardium. *J. Physiol.* (*Lond.*). 302:131–153.

Rieser, G., R. Sabbadini, P. Paolini, M. Fry, and G. Inesi. 1979. Sarcomere motion in isolated cardiac cells. *Am. J. Physiol.* 236:C70–C77.

Roos, K. P., R. J. Baskin, R. L. Lieber, J. W. Cline, and P. J. Paolini. 1980. Digital data acquisition and analysis of striated muscle diffraction patterns with a direct memory access microprocessor system. *Rev. Sci. Instrum.* 51:762–767.

Roos, K. P., A. J. Brady, and S. T. Tan. 1982. The direct measurement of sarcomere length from isolated cardiac cells. *Am. J. Physiol.* 242:H68–H78.

Rudel, R., and F. Zite-Ferenczy. 1979. Interpretation of light diffraction by cross-striated muscle as Bragg reflexion of light by the lattice of contractile proteins. *J. Physiol.* (*Lond.*). 290:317–330.

Smith, W. J. 1966. Modern Optical Engineering - the Design of Optical Systems. McGraw-Hill, Inc., New York. 476.

Walraven, R. 1980. Digital filters. *Proc. Digital Equip. Comp. Users Soc.* 1:827–833.

Walter, R. J., and M. W. Berns. 1981. Computer-enhanced video microscopy digitally processed microscope images can be produced in real time. *Proc. Natl. Acad. Sci. U. S. A.* 78:6927–6931.

Wittenberg, B. A., and T. F. Robinson. 1981. Oxygen requirement, morphology cell coat, and membrane permeability of calcium-tolerant myocytes from hearts of adult rats. *Cell Tissue Res.* 216:231–251.